Continuous GNSS-RTK Aided by LiDAR/Inertial Odometry with Intelligent GNSS Selection in Urban Canyons

Jiachen Zhang[1,2], Weisong Wen[2] , Feng Huang[2] , Xiaodong Chen[1] and Li-Ta Hsu[2]
[1]*School of Precision Instrument and Opto-electronics Engineering, Tianjin University*
[2]*Department of Aeronautical and Aviation Engineering, the Hong Kong Polytechnic University*

BIOGRAPHY

Jiachen Zhang received her bachelor's degree from Tianjin University in Information Engineering in 2016 and is currently an enrolled, full-time Ph.D. candidate at Tianjin University, majoring in Optical Engineering. She is working as a research assistant in the Intelligent Positioning and Navigation Laboratory. Her research interests including localization and sensor-fusion for autonomous driving.

Weisong Wen was born in Ganzhou, Jiangxi, China. He received a Ph.D. degree in mechanical engineering, the Hong Kong Polytechnic University, in 2020. He is currently a research assistant professor at the Hong Kong Polytechnic University. His research interests include multi-sensor integrated localization for autonomous vehicles, SLAM, and GNSS positioning in urban canyons. He was a visiting student researcher at the University of California, Berkeley (UCB) in 2018.

Feng Huang received his bachelor's degree from Shenzhen University in Automation in 2014 and MSc in Electronic Engineering at Hong Kong University of Science and Technology in 2016. He is a Ph.D. student in the Department of Aeronautical and Aviation Engineering, Hong Kong Polytechnic University. His research interests including localization and sensor fusion for autonomous driving.

Xiaodong Chen received the B.S. and Ph.D. degrees in Optical Engineering from TianJin University in 1996 and 2001. He is currently a professor with the School of Precision Instruments and Opto-Electronic Engineering, Tianjin University. In 2009 and 2011, he went to Oklahoma University for cooperative study and participated in two NIH R01 projects. His research interests include photoelectric detection, medical image processing, and computer vision.

Li-Ta Hsu received the B.S. and Ph.D. degrees in aeronautics and astronautics from National Cheng Kung University, Taiwan, in 2007 and 2013, respectively. He is currently an assistant professor with the Division of Aeronautical and Aviation Engineering, Hong Kong Polytechnic University, before he served as post-doctoral researcher in Institute of Industrial Science at University of Tokyo, Japan. In 2012, he was a visiting scholar in University College London, U.K. He was a technical representative in ION in 2019-2021 and is an Associate Fellow of RIN. His research interests include GNSS positioning in challenging environments and localization for pedestrian, autonomous driving vehicle and unmanned aerial vehicle.

ABSTRACT

Accurate and globally referenced positioning is the key prerequisite for fully successful autonomous systems. Global Navigation Satellite System (GNSS) could provide global positioning service in open areas. Unfortunately, under denes urban areas, in which it is typical for autonomous systems to operate, the performance of GNSS suffers from non-line-of-sight (NLOS) receptions and multipath effects caused by GNSS signal reflection and blockage from surrounding buildings. Thus, it will lead to position measurements with terribly large errors and GNSS outage. To facilitate long-term stable and accurate navigation, this paper proposes a method of continuous GNSS Real-time Kinematic (RTK) positioning aided by he 3D light detection and ranging (LiDAR) /inertial odometry (LIO) with intelligent GNSS selection in urban canyons. The coarse-to-fine LIO keeps on generating a

 https://doi.org/10.33012/2021.18089

locally accurate motion estimation and a registered point cloud map. Inspired by the outstanding capability of the environmental description of 3D LiDAR, available GNSS-RTK under light urban environment is detected as the degree of urbanization is evaluated via the sky-mask elevation angle calculation, which will be further integrated with the relative motion estimation from LIO based on factor graph optimization. Therefore, the continuous and accurate positioning is guaranteed by the local estimation from low-drift LIO in highly urbanized areas and global correction once the "Available GNSS-RTK" is obtained. The experimental results in a typical urban canyon in Hong Kong shows that the performance of the proposed integration pipeline is significantly improved in comparison with that without GNSS-RTK selection.

1. INTRODUCTION

Accurate and globally referenced positioning is the key prerequisite for fully successful autonomous systems, such as unmanned ground vehicles [1] and outdoor mobile robots. As well known, centimeter-level positioning accuracy can be achieved based on the double-differential carrier and code measurements in the open area when the fixed Global Navigation Satellite System (GNSS) Real-time Kinematic (RTK) solution is achieved. However, it is typical for autonomous systems to operate in both open areas and urban canyons. Unfortunately, under denes urban areas, the performance of GNSS-RTK suffers from non-line-of-sight (NLOS) receptions and multipath effects caused by GNSS signal reflection and blockage from surrounding buildings [2], which will lead to outliers with terribly large errors. In short, the major challenge of GNSS-RTK is that accuracy is not guaranteed in urban canyons.

To fill this gap, the integration of the GNSS-RTK and inertial measurement unit (IMU) was widely studied due to their complementariness to guarantee the positioning accuracy in urban canyons. [3] proposed tightly coupled integration of the single-frequency multi-GNSS RTK and low-cost IMU. Via outlier-resistant ambiguity resolution and Kalman filter strategy, the fixing rate was improved by about 10%. However, the residual-based outlier rejection easily caused false negative judgement and the performance relies heavily on the cost of the IMU sensor for long GNSS outage durations.

The 3D light detection and ranging (LiDAR), which produces high-precision and long-range distance measurements that are reliable due to active detection and illumination invariance property, becomes available and plays a significant role in the fully autonomous driving vehicle. It's commonly used to provide locally accurate relative positioning in a short period in structured scenarios with adequate features [4]. However, our previous work in [5] showed that the performance of LiDAR odometry can be significantly challenged in urban canyons due to the numerous unexpected dynamic objects. To alleviate this problem, our recent work in [6] proposed a coarse-to-fine LiDAR/inertial odometry by combining the IMU and 3D LiDAR which led to robust and accurate odometry. Undoubtedly, the combination of the GNSS-RTK, IMU, and 3D LiDAR is a promising solution to provide locally accurate (take advantage of LiDAR inertial odometry) and free-of-drift absolute positioning (take advantage of GNSS-RTK). The work in [7] proposed to directly integrate the measurements from GNSS-RTK, IMU, and 3D LiDAR via factor graph optimization. Nevertheless, the quality levels of the three kinds of applied measurements are different in different scenarios. In open areas, the direct combination of the sensor sources can lead to centimeter positioning accuracy. While in GNSS denied environments, such as urban canyons, the measurements of GNSS-RTK are highly unreliable with meter-level error [8]. Degraded GNSS RTK solutions distort the accuracy of LiDAR/IMU odometry. How to select the good GNSS-RTK positioning measurements before its integration with the 3D LiDAR and IMU is the bottleneck for the loosely coupled GNSS-RTK/IMU/LiDAR fusion.

To facilitate long-term stable and accurate navigation, this paper proposes a method of continuous GNSS-RTK positioning aided by LiDAR/inertial odometry with intelligent GNSS selection in urban canyons. The major contribution expands from the following aspects:

1) An intelligent available GNSS-RTK selection method is developed exploiting the registered 3D point map generated by LiDAR/inertial odometry.
2) A loosely coupled available-GNSS-RTK/LiDAR/inertial integration pipeline based on factor graph optimization (FGO) [9] is implemented to achieve absolute positioning in urban canyons.
3) Verification of the proposed method is conducted on typical urban areas in Hong Kong. Precision of position estimation is improved compared with the pipelines that integrate all the received GNSS-RTK with LiDAR/inertial odometry.

The rest of the paper is arranged as follows: Section 2 present the proposed method in detail. Section 3 shows the qualitative and quantitative evaluation of the proposed method. Section 4 will summarize the work and make future perspectives.

2. METHODOLOGY

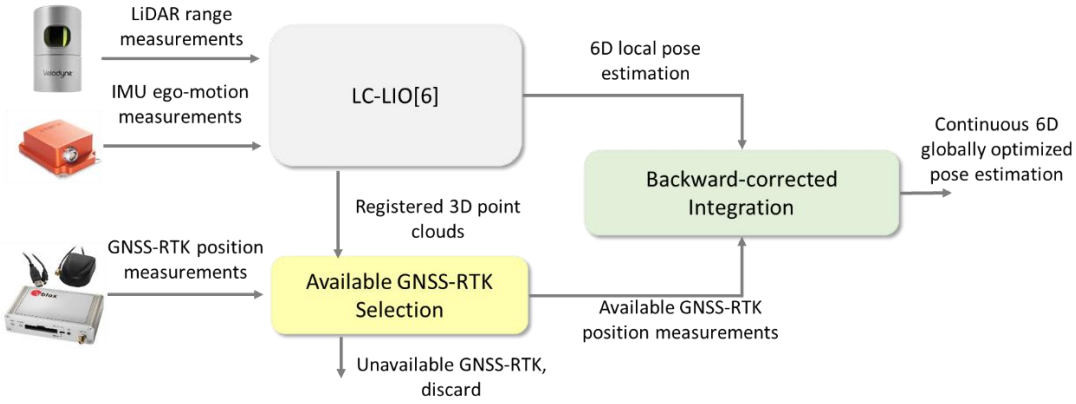

Fig. 1 The overview of the proposed pipeline.

The overview of the proposed pipeline is presented in Fig. 1. There are three kinds of inputs, LiDAR range measurements, IMU ego-motion measurements and GNSS-RTK position measurements. Firstly, the LiDAR/inertial odometry implemented as our previous work LC-LIO [6] generates a locally accurate 6D motion estimation and a registered point cloud map continuously. In LC-LIO [6], LiDAR and IMU measurement modeling is accomplished via feature-based scan-to-map registration [4] and pre-integration [10] respectively. The two modeling procedures proceed separately. Joint FGO [9] of motion estimation from the two procedures is performed then. Optimized results provide an initial guess to improve the registration. Besides, it will correct the bias of the accelerometer and gyroscope for accurate pre-integration. For more details our previously published work [6] are recommended. Secondly, with the assistance of the registered 3D point cloud map, the available GNSS-RTK Selection module discard unavailable GNSS RTK and preserve available GNSS-RTK position measurements, which are more likely to be in deep urban canyons and light urban environments respectively. Finally, during backward-corrected integration based on FGO [9] between available GNSS-RTK and relative pose from LC-LIO, the Continuous 6D globally optimized pose estimation is achieved.

2.1 Available GNSS-RTK Selection

Intuitively, the large sky-mask elevation angle indicates high-rising buildings around or obstruction overhead [11] where the GNSS-RTK solutions are supposed to be unavailable. On the contrary, the small sky-mask elevation angle indicates open area [11]. The GNSS-RTK solution are supposed to be available. According to this concept, available GNSS-RTK selection is implemented via three steps described in Fig. 2.

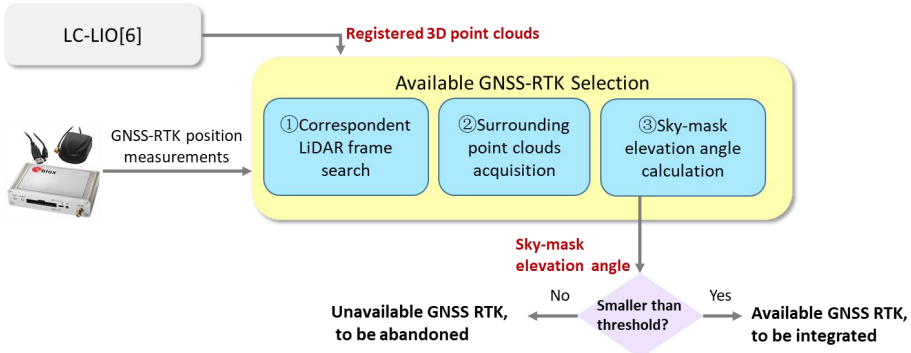

Fig. 2 Detailed steps of "Available GNSS-RTK Selection"

At first, for each input GNSS-RTK, we find its correspondent LiDAR frame, which is composed of registered 3D point clouds at one sweep, according to the time synchronized by ROS [12]. Then backward and forward surrounding point clouds of the correspondent LiDAR frame is acquired according to predefined range parameters as shown in Fig. 3 (a). In the horizontal

direction, 50 meters for both sides are selected in our implementation. The generated local point cloud map describing the surroundings around the current GNSS-RTK solution as shown in Fig. 3 (b) are employed to evaluate the sky-mask elevation angle.

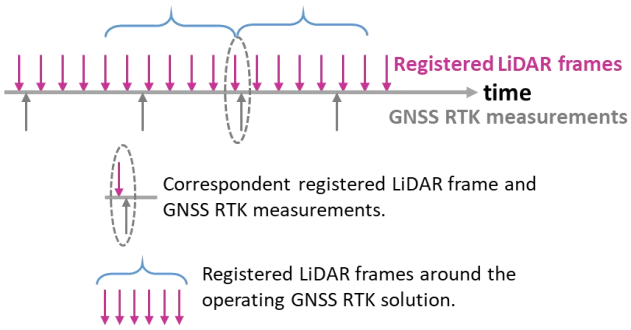

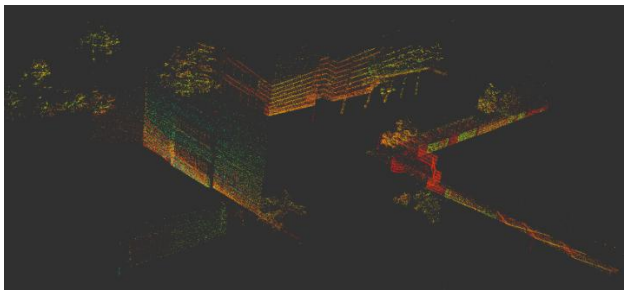

(a) **(b)**

Fig. 3 (a) Correspondent LiDAR frame search and surrounding point clouds acquisition of the operating GNSS-RTK. (b) An instance of point clouds acquired according to the proposed method for sky-mask elevation angle calculation of the operating GNSS-RTK on the UrbanNav-HK-Data20190428 [13]

For sky-mask elevation angle calculation 360 degrees, that is 360 directions, around the k_th operating GNSS-RTK $\mathbf{gr}_k$ is taken into consideration as shown in Fig. 4 (a) with each direction denoted as $d_i, i \in [1,2,\cdots,360]$. There is 1º between d_i and d_{i+1}. Each registered 3D point is categorized into a direction according to its azimuth angle derived from the coordinates provided by LC-LIO [6]. Take the direction d_i as an example, all possible elevation angles generated by the 3D points at this direction are denoted as $e_{d_i,1}, e_{d_i,2}, \cdots, e_{d_i,n}$ and $e_{d_i,n}$ with n representing the index of a 3D point is calculated as follow:

$$e_{d_i,n} = \arctan\left(\frac{y_{d_i,n}}{x_{d_i,n}}\right) \#(1)$$

In which $y_{d_i,n}$ and $x_{d_i,n}$ are the coordinates of the n_th 3D point as shown in Fig. 4 (b). The final sky-mask elevation angle e_{d_i} at d_i is defined as the maximum one among all the possible angles:

$$e_{d_i} = \max\{e_{d_i,1}, e_{d_i,2}, \cdots, e_{d_i,n}\} \#(2)$$

The sky-mask elevation angle $e_{\boldsymbol{GR_k}}$ of $\mathbf{gr}_k$ is defined as the mean of that at all the directions[11]:

$$e_{\boldsymbol{GR_k}} = \frac{1}{360}\sum_{i=1,\cdots,360} e_{d_i} \#(3)$$

As mentioned earlier, $\mathbf{gr}_k$ with $e_{\boldsymbol{GR_k}}$ larger than the predefined threshold is regarded as unavailable GNSS-RTK while the opposite ones are selected as available GNSS-RTK for further integration.

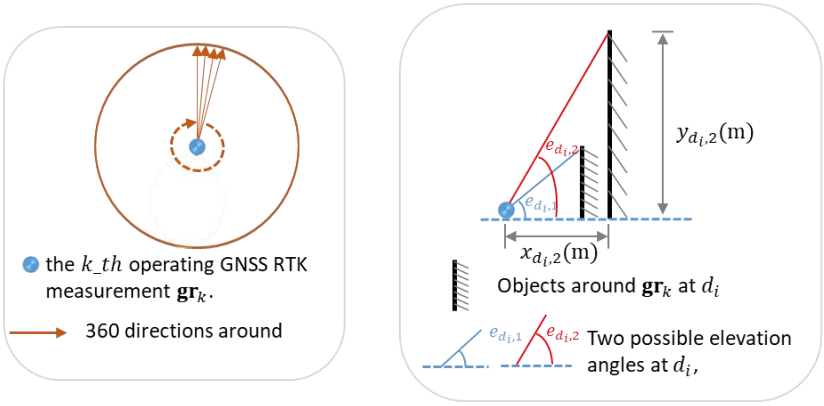

(a) **(b)**

Fig. 4 Sky-mask elevation angle calculation. (a) The top view of the 360 directions around the operating GNSS-RTK measurement $\mathbf{gr}_k$. (b) Take the direction d_i as an example, front view of all the possible elevation angles at d_i. The objects are described by registered 3D point clouds from LC-LIO[6].

2.2 Backward-Corrected Integration

To achieve globally accurate position estimation, integration of available GNSS-RTK and relative 6D motion estimation from LC-LIO [6] is performed based on FGO [9]. For clarity, coordinate frames employed later is defined as follows:

1) The LiDAR body frame: $\{\cdot\}^L$, fixed at the center of the LiDAR sensor.
2) The LiDAR world frame: $\{\cdot\}^{L_0}$, the initial LiDAR body frame.
3) The local ENU frame : $\{\cdot\}^W$, the ENU frame originated at the start position.

The transformation matrix from the local ENU frame to the LiDAR world frame is pre-calibrated and represented as follows:

$$\mathbf{T}_W^{L_0} = \begin{bmatrix} \mathbf{R}_W^{L_0} & \mathbf{p}_W^{L_0} \\ 0 & 1 \end{bmatrix} \in SE(3) \# (4)$$

In which, $\mathbf{p}_W^{L_0} \in R^3$ is the position and $\mathbf{R}_W^{L_0} \in SO(3)$ is the rotation matrix [14].

The factor graph of the optimization is depicted in Fig. 5. The states to be estimated are 6D poses at LiDAR timestamps, with each of them expressed as the compound vector of translation and quaternion [15]:

$$\mathbf{X} = \{\boldsymbol{x}_0, \boldsymbol{x}_1, \boldsymbol{x}_2, \cdots, \boldsymbol{x}_i, \cdots \boldsymbol{x}_n\}, \boldsymbol{x}_i = \left[\boldsymbol{p}_i^W, \ \boldsymbol{q}_i^W\right] \# (5)$$

In which, n is the number of states. $\boldsymbol{p}_i^W = [x_i^W, y_i^W, z_i^W]^T \in R^3$ and $\boldsymbol{q}_i^W$ represents the position and the rotation in quaternion form respectively. One of the two kinds of measurements used to construct the factors is relative 6D motion estimation $\mathbf{T}_{L_i}^W$ from LC-LIO [6] defined as:

$$\mathbf{T}_{L_i}^W = \begin{bmatrix} \mathbf{R}_{L_i}^{L_0} & \boldsymbol{p}_{L_i}^{L_0} \\ 0 & 1 \end{bmatrix} \in SE(3) \# (6)$$

In which i is the index of LiDAR frame. $\boldsymbol{p}_{L_i}^{L_0} \in R^3$ is the relative position and $\mathbf{R}_{L_i}^{L_0} \in SO(3)$ represents the rotation matrix. The other kind of measurements used to construct the factors is 2D available GNSS-RTK solutions denoted as

$$\tilde{\boldsymbol{p}}_j^W = \left[\tilde{x}_j^W, \tilde{y}_j^W\right]^T \in R^2, \ j \in [0, m] \# (7)$$

In which m is the number of available GNSS-RTK solutions. It's considered that in urban areas the z component of the commercial grade GNSS-RTK solution tends to be unreliable compared with the x and y component and thus not used during the integration.

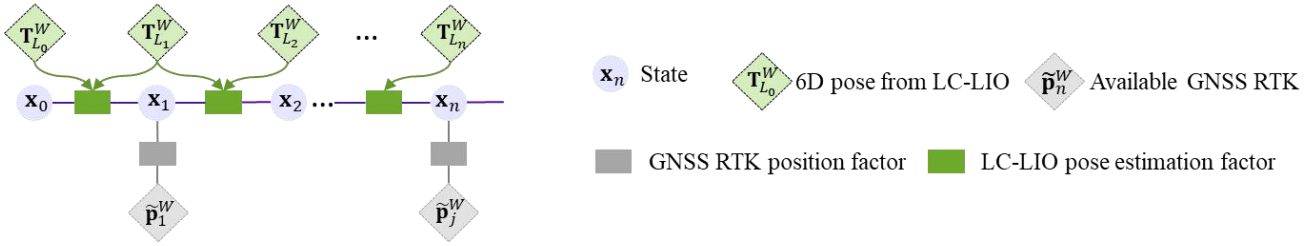

Fig. 5 Factor graph of backward-corrected integration of available GNSS-RTK and relative 6D motion estimation from LC-LIO[6]

As shown in Fig. 5, two kinds of factors constrain the states during the optimization. The first one is LC-LIO pose estimation factor depicted in green. The residuals are defined as the relative pose error as follows:

$$\mathbf{r}_{\mathcal{L}}\left(\mathbf{T}_{L_i}^{L_0},\mathbf{X}\right)=\left(\mathbf{T}_{L_{i-1}}^{L_0}{}^{-1}\mathbf{T}_{L_i}^{L_0}\right)^{-1}\ominus\left(\boldsymbol{x}_{i-1}{}^{-1}\otimes\boldsymbol{x}_i\right)\#(8)$$

In which, $\otimes$ and $\ominus$ represent the generalized 6D pose multiplication rules with rotation in the quaternion format [15].The other one is GNSS RTK position factor depicted in gray. The residuals are defined as the absolute 2D translation error as follows:

$$\mathbf{r}_{\mathcal{G}}\left(\widetilde{\boldsymbol{p}}_j^W,\mathbf{X}\right)=\mathbf{T}_W^{L_0}\widetilde{\boldsymbol{p}}_j^W-\boldsymbol{p}_i^W\#(9)$$

The objective function could be defined as follows:

$$\mathbf{X}=\min_{\mathbf{X}}\frac{1}{2}\left\{\sum_{i\in\{0,\cdots,n\}}\rho\left(\left\|\mathbf{r}_{\mathcal{L}}\left(\mathbf{T}_{L_i}^{L_0},\mathbf{X}\right)\right\|_{\mathbf{C}_{L_i}}^2\right)+\sum_{j\in\{0,\cdots,m\}}\rho\left(\left\|\mathbf{r}_{\mathcal{G}}\left(\widetilde{\boldsymbol{p}}_j^W,\mathbf{X}\right)\right\|_{\mathbf{C}_{\widetilde{\boldsymbol{p}}_j^W}}^2\right)\right\}\#(10)$$

In which $\mathbf{C}_{L_i}$ and $\mathbf{C}_{\widetilde{\boldsymbol{p}}_j^W}$ is the fixed information matrix for $\mathbf{r}_{\mathcal{L}}\left(\mathbf{T}_{L_i}^{L_0},\mathbf{X}\right)$ and $\mathbf{r}_{\mathcal{G}}\left(\widetilde{\boldsymbol{p}}_j^W,\mathbf{X}\right)$ respectively with 0.1 for the translation part and 0.01 for the rotation part. $\rho(\cdot)$ is the Cauchy kernel [16] for outlier suppression defined as:

$$\rho(s)=c^2\log\left(1+\frac{s}{c^2}\right)\#(11)$$

In which c is the control parameter set to 1 [17]. The Levenberg-Marquardt (L-M) algorithm [18] implemented in Ceres Solver [19] is employed to solve the nonlinear optimization problem. Each available GNSS-RTK solution would invoke the global optimization of all the states backward from it. Continuous and globally optimized position is finally achieved.

3. EXPERIMENTAL RESULTS

3.1 Sensor Setup

The experiment was conducted in typical urban canyons in Hong Kong to verify the effectiveness of the proposed method. The UrbanNav dataset (https://github.com/IPNL-POLYU/UrbanNavDataset, accessed on 20 September 2021) [13] is open to the community for further algorithm development and verification. As shown in Fig. 6 (a) and Fig. 6 (b), a commercial-level u-blox M8T GNSS receiver was used to collect the GNSS-RTK solution. The Velodyne HDL-32E was employed to collect raw 3D point clouds at a frequency of 10 Hz. The Xsens Ti-10 IMU was employed to collect acceleration and angular velocity at a frequency of 200 Hz. Besides, the NovAtel SPAN-CPT, a GNSS (GPS, GLONASS, and Beidou) RTK/INS (fiber-optic gyroscopes, FOG) integrated navigation system was used to provide ground truth of positioning. All the data were collected and synchronized using a robot operation system (ROS) [12]. The coordinate systems among all the sensors were calibrated in advance. Fig. 6 (c) depicts the ground truth on Google Earth of the UrbanNav-HK-Data-20190428 used in the experiment.

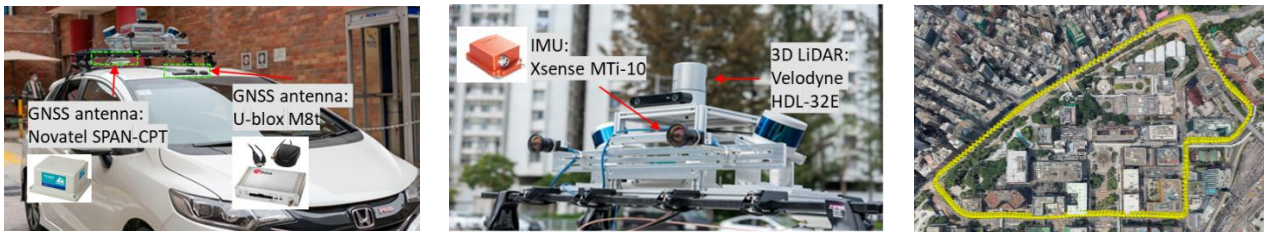

(a) (b) (c)

Fig. 6 (a) and (b) Sensor setup used when the UrbanNav-HK-Data was collected. (c) The ground truth of the UrbanNav-HK-Data-20190428 aligned on Google Earth from the bird-eye view

During the evaluation, the following three pipelines are compared:

1) GLI-FULL: The conventional method which loosely fuse all the received GNSS-RTK with LC-LIO.
2) GLI-35º: The proposed method which loosely fuse available GNSS-RTK with LC-LIO with the sky-mask value threshold for selection set to 35º.
3) GLI-15º: The proposed method which loosely fuse available GNSS-RTK with LC-LIO with the sky-mask value threshold for selection set to 15º.

The results are quantitatively evaluated by 3D absolute translation error (ATE) implemented in EVO[20].

3.2 Generated Sky-mask Elevation Angle Results On the UrbanNav-HK-Data-20190428

The sky-mask elevation angle results and the ATE of the GNSS-RTK solutions produced by the u-blox M8T are plot in Fig. 7. At most cases, large sky-mask elevation angle indicating deep urban canyons around are accompanied by large ATE as we expected such as the ① place. Small sky-mask elevation angle indicating light urban environment around are accompanied by small ATE as we expected such as the ② place. However, false detection of unavailable GNSS-RTK solutions under relatively open areas occur effected by trees, streetlights and etc. such as the ③ place. Adaptive or multi-layer thresholds would be further implemented for robustness improvement when selecting available GNSS RTK.

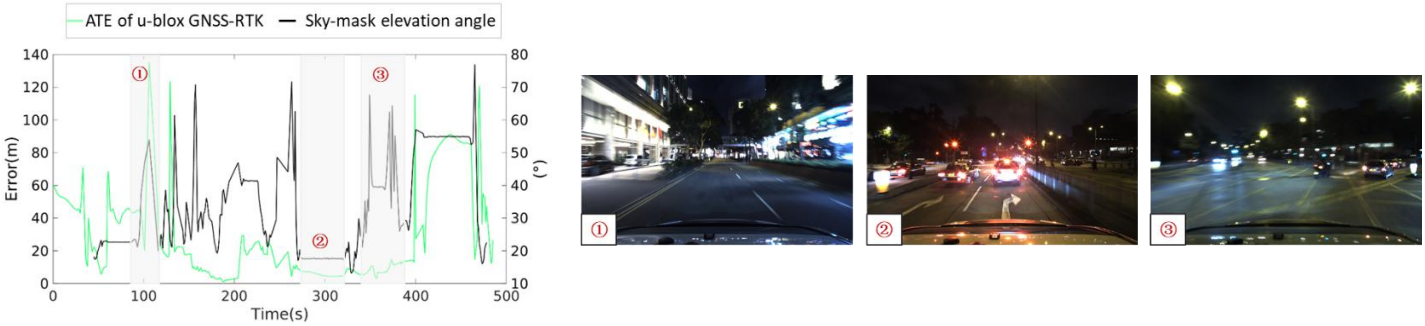

Fig. 7 The sky-mask elevation angle results and the ATE of the GNSS-RTK solutions produced by the u-blox M8T. At the ① place, pedestrian overpass ahead and high-rise buildings on both sides results in large sky-mask elevation angle and poor position measurements with large ATE. At the ② place, an open intersection, small sky-mask elevation angle and good position measurements with small ATE are achieved. At the ③ place, an open intersection, the position measurements are relatively good with small ATE. While the streetlights above the car detected by LiDAR results in large sky-mask elevation angle.

3.3 The Qualitative Comparison of GLI-FULL, GLI-35º and GLI-15º

The trajectory generated by GLI-FULL, GLI-35º and GLI-15º with the error mapped on are plot in Fig. 8. GLI-FULL loosely fused all the received GNSS-RTK with LC-LIO during when unavailable GNSS-RTK solutions with large error destroy the estimation, and thus produces the worst trajectory as shown in Fig. 8 (a). GLI 35º and GLI 15º fuse the GNSS-RTK solutions of which the sky-mask elevation angles are less than 35º and 15º respectively with LC-LIO. The trajectories are significantly more precise compared with that of GLI-FULL which proved the effectiveness of the proposed integration method. In addition, the smaller threshold for

available GNSS-RTK selection rejects more unavailable ones therefore leads to more accurate position estimation. As shown in Fig. 8 (b) and Fig. 8 (c), the trajectory produced by GLI 15º overlap with the ground truth much better compared with that of GLI 35º.

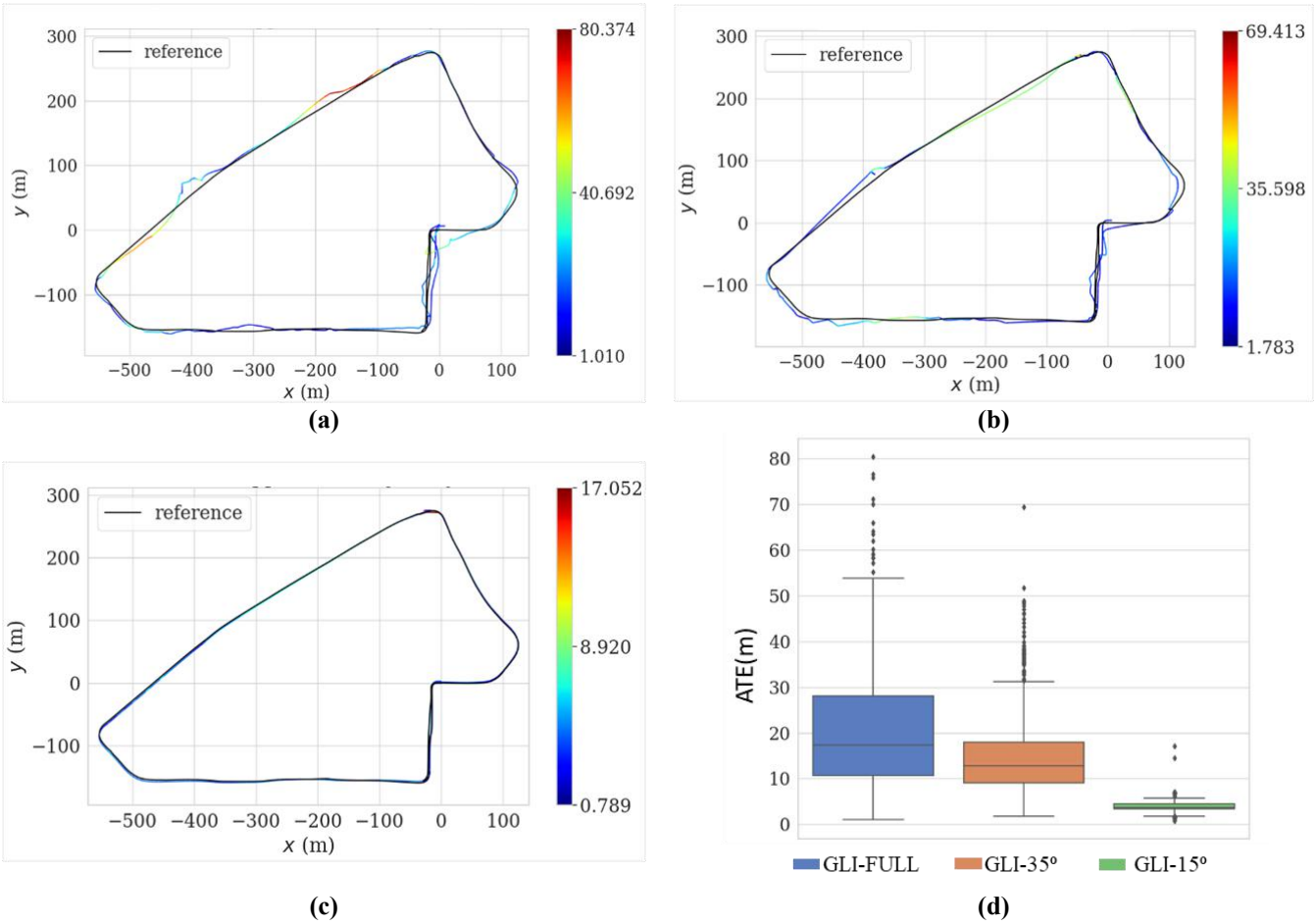

Fig. 8 (a), (b), and (c) plots the trajectory generated by GLI-FULL, GLI-35º and GLI-15º with the ATE (m) mapped on respectively. The color bar represents different ATE (m) values painted on the estimated trajectory. The black trajectory denoted as reference are the ground truth. (d) shows the boxplot of the ATE (m) on the whole trajectory produced by the three pipelines.

3.4 The Quantitative Comparison of GLI-FULL, GLI-35º and GLI-15º

Table 1 shows the mean and Root Mean Square Error (RMSE) of the 3D ATE of the trajectory estimated by GLI-FULL, GLI-35º, and GLI-15º. For GLI-FULL, the mean ATE is 20.90m with a RMSE of 17.41m. By GLI-35º, a 25% improved mean ATE of 15.75m and a 27% improved RMSE of 12.76m is achieved. The improvement indicates the superiority of the proposed integration framework. GLI-15º achieves best precision with the mean ATE of 3.87 m and the RMSE of 3.64 m as marked in bold font. Via minifying the threshold, the effectiveness of the available GNSS-RTK selection method is validated. Nevertheless, the precision of GLI-15º is still at meter-level which is not capable of demanding navigation task due to the accumulated drift of the LiDAR/inertial odometry on the vertical directions and the large error of GNSS measurements provided by commercial level receivers.

Table 1. ATE of the trajectory estimated by GLI-FULL, GLI-35º, and GLI-15º with the bold values representing the best precision.

Dataset	Method	ATE (m)	
		Mean	RMSE
UrbanNav-HK-Data20190428	GLI-FULL	20.90	17.41
	GLI-35º	15.75	12.76
	GLI-15º	**3.87**	**3.64**

4. CONCLUSIONS AND FUTURE PERSPECTIVES

This paper put forward an intelligent available GNSS-RTK selection method exploiting the registered 3D point map produced by LiDAR/IMU odometry. The available-GNSS-RTK/LiDAR/Inertial loosely coupled pipeline based on FGO achieves continuous global positioning in urban canyons. The ATE of the proposed method is significantly improved compared with the pipeline that loosely coupled all the received GNSS-RTK measurements.

For further study, we would implement adaptive threshold for available GNSS-RTK selection to improve the robustness. Moreover, cameras or wheel encoders would be employed to enhance the precision of the relative pose estimation[21, 22]. Last but not least, verification on more urban datasets [13] especially that with more accurate GNSS measurements will be conducted.

5. REFERENCES

[1] G. Wan *et al.*, "Robust and precise vehicle localization based on multi-sensor fusion in diverse city scenes," in *2018 IEEE International Conference on Robotics and Automation (ICRA)*, 2018, pp. 4670-4677: IEEE.

[2] L.-T. Hsu, "Analysis and modeling GPS NLOS effect in highly urbanized area," *GPS solutions,* vol. 22, no. 1, pp. 1-12, 2018.

[3] T. Li, H. Zhang, Z. Gao, Q. Chen, and X. Niu, "High-accuracy positioning in urban environments using single-frequency multi-GNSS RTK/MEMS-IMU integration," *Remote sensing,* vol. 10, no. 2, p. 205, 2018.

[4] J. Zhang and S. Singh, "Low-drift and real-time lidar odometry and mapping," *Autonomous Robots,* vol. 41, no. 2, pp. 401-416, 2017.

[5] W. Wen, L.-T. Hsu, and G. Zhang, "Performance analysis of NDT-based graph SLAM for autonomous vehicle in diverse typical driving scenarios of Hong Kong," *Sensors,* vol. 18, no. 11, p. 3928, 2018.

[6] J. Zhang, W. Wen, F. Huang, X. Chen, and L.-T. Hsu, "Coarse-to-Fine Loosely-Coupled LiDAR-Inertial Odometry for Urban Positioning and Mapping," *Remote Sensing,* vol. 13, no. 12, p. 2371, 2021.

[7] L. Chang, X. Niu, T. Liu, J. Tang, and C. Qian, "GNSS/INS/LiDAR-SLAM integrated navigation system based on graph optimization," *Remote Sensing,* vol. 11, no. 9, p. 1009, 2019.

[8] P. D. Groves, "Principles of GNSS, inertial, and multisensor integrated navigation systems, [Book review]," *IEEE Aerospace and Electronic Systems Magazine,* vol. 30, no. 2, pp. 26-27, 2015.

[9] F. Dellaert and M. Kaess, "Factor graphs for robot perception," *Foundations Trends® in Robotics,* vol. 6, no. 1-2, pp. 1-139, 2017.

[10] C. Forster, L. Carlone, F. Dellaert, and D. Scaramuzza, "On-Manifold Preintegration for Real-Time Visual--Inertial Odometry," *IEEE Transactions on Robotics,* vol. 33, no. 1, pp. 1-21, 2016.

[11] W. Wen *et al.*, "Urbanloco: a full sensor suite dataset for mapping and localization in urban scenes," in *2020 IEEE International Conference on Robotics and Automation (ICRA)*, 2020, pp. 2310-2316: IEEE.

[12] M. Quigley *et al.*, "ROS: an open-source Robot Operating System," in *ICRA workshop on open source software*, Kobe, Japan, 2009, vol. 3, no. 3.2, p. 5.

[13] L.-T. Hsu, N. Kubo, W. Chen, Z. Liu, T. Suzuki, and J. Meguro, "UrbanNav:An open-sourced multisensory dataset for benchmarking positioning algorithms designed for urban areas (Accepted)," in *ION GNSS+ 2021*, Saint Louis, Mississippi, 2021.

[14] T. D. Barfoot, *State Estimation for Robotics*. Cambridge: Cambridge University Press, 2017, pp. 205-284.

[15] J. C. Chou, "Quaternion kinematic and dynamic differential equations," *IEEE Transactions on robotics and automation,* vol. 8, no. 1, pp. 53-64, 1992.

[16] Z. Zhang, "Parameter estimation techniques: A tutorial with application to conic fitting," *Image vision Computing,* vol. 15, no. 1, pp. 59-76, 1997.
[17] G. Hu, K. Khosoussi, and S. Huang, "Towards a reliable SLAM back-end," in *2013 IEEE/RSJ International Conference on Intelligent Robots and Systems*, Tokyo, Japan, 2013, pp. 37-43: IEEE.
[18] J. J. Moré, "The Levenberg-Marquardt algorithm: implementation and theory," in *Numerical analysis*: Springer, 1978, pp. 105-116.
[19] S. Agarwal and K. Mierle. (6 January 2021). *Ceres Solver*. Available: http://ceres-solver.org
[20] M. Grupp. (2017, 01 03 2021). *evo: Python package for the evaluation of odometry and SLAM.* Available: https://github.com/MichaelGrupp/evo
[21] T. Shan, B. Englot, C. Ratti, and D. Rus, "LVI-SAM: Tightly-coupled Lidar-Visual-Inertial Odometry via Smoothing and Mapping," in *IEEE International Conference on Robotics and Automation (ICRA)*, 2021: IEEE.
[22] K. J. Wu, C. X. Guo, G. Georgiou, and S. I. Roumeliotis, "Vins on wheels," in *2017 IEEE International Conference on Robotics and Automation (ICRA)*, 2017, pp. 5155-5162: IEEE.